Supplement of Atmos. Chem. Phys., 22, 9129–9160, 2022
https://doi.org/10.5194/acp-22-9129-2022-supplement

Atmospheric Chemistry and Physics
Open Access
EGU

Supplement of

Effective radiative forcing of anthropogenic aerosols in E3SM version 1: historical changes, causality, decomposition, and parameterization sensitivities

Kai Zhang et al.

Correspondence to: K. Zhang (kai.zhang@pnnl.gov)

1 List of supplemental figures

- Figure S1: As Figure 8, but for the NH polar region.
- Figure S2: As Figure 8, but for the NH mid-latitude region.
- Figure S3: As Figure 8, but for the tropics.
- Figure S4: As Figure 9, but for relationships between ΔN_i and N_i, and between relative changes in N_i and other quantities.
- Figure S5: Annual mean global distribution of anthropogenic aerosol effects ($W\,m^{-2}$) estimated with year 2000 CMIP5 (2nd row) and CMIP6 (1st row) emissions.
- Figure S6: Annual mean global distribution of liquid water path and the sensitivity to aerosol perturbations ($W\,m^{-2}$) in the reference and sensitivity simulations.
- Figure S7: Annual mean global distribution of ice water path and the sensitivity to aerosol perturbations ($W\,m^{-2}$) in the reference and sensitivity simulations.
- Figure S8: Annual mean global distribution of AOD in simulations with emissions for different years.
- Figure S9: Annual mean global distribution of column-integrated CCN (at 0.1% supersaturation) concentrations in simulations with emissions for different years.
- Figure S10: Annual mean global distribution of column-integrated cloud droplet number concentrations (N_d) in simulations with emissions for different years.
- Figure S11: Similar as Figure S10, but annual mean global distribution of ice crystal number concentrations (N_i) vertically-integrated above 300hPa in simulations with emissions for different years.

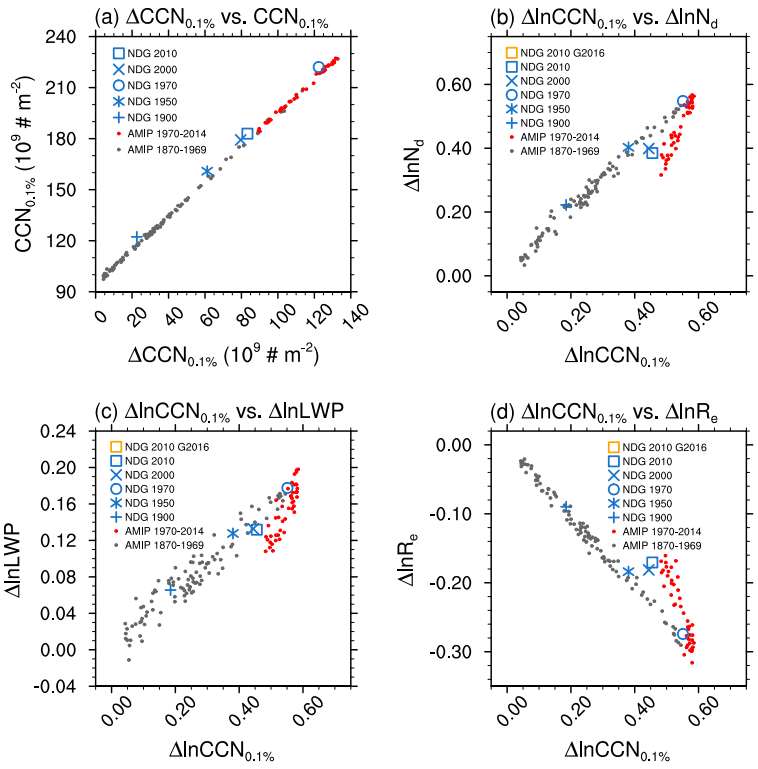

Figure S1: As Figure 8, but for the NH polar region. See section 4.2 for details.

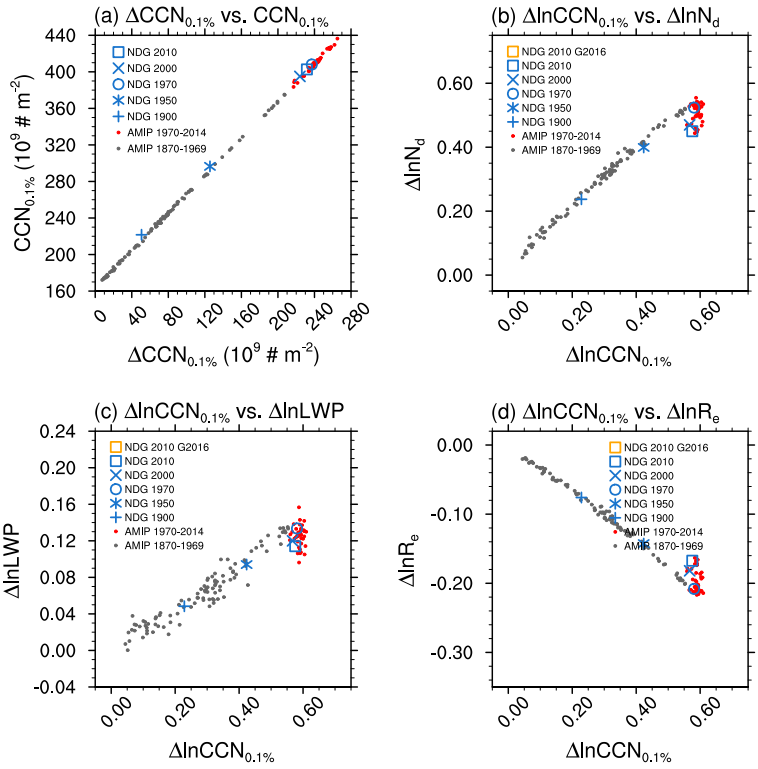

Figure S2: As Figure 8, but for the NH mid-latitude region. See section 4.2 for details.

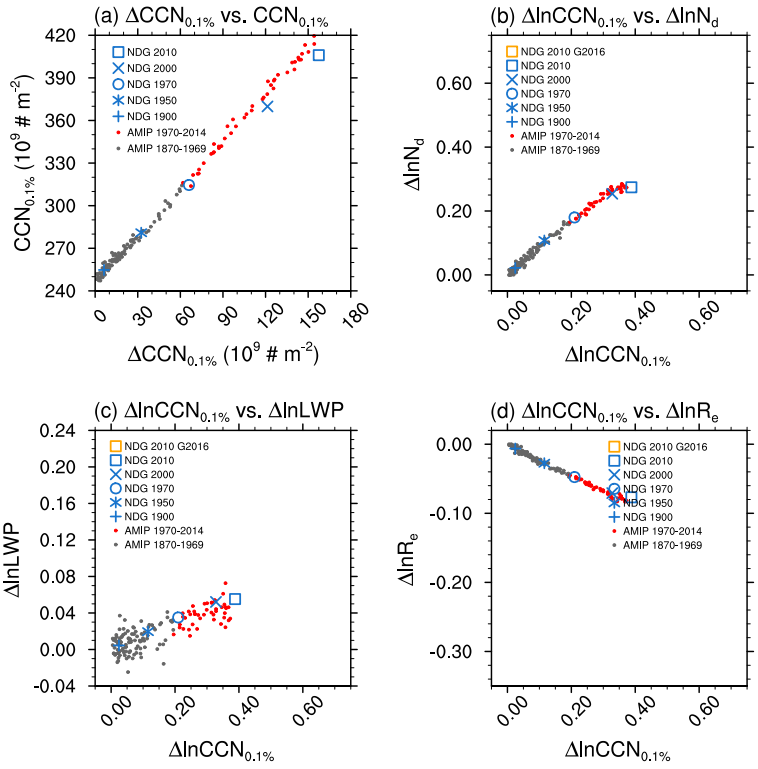

Figure S3: Figure 8, but for the tropics. See section 4.2 for details.

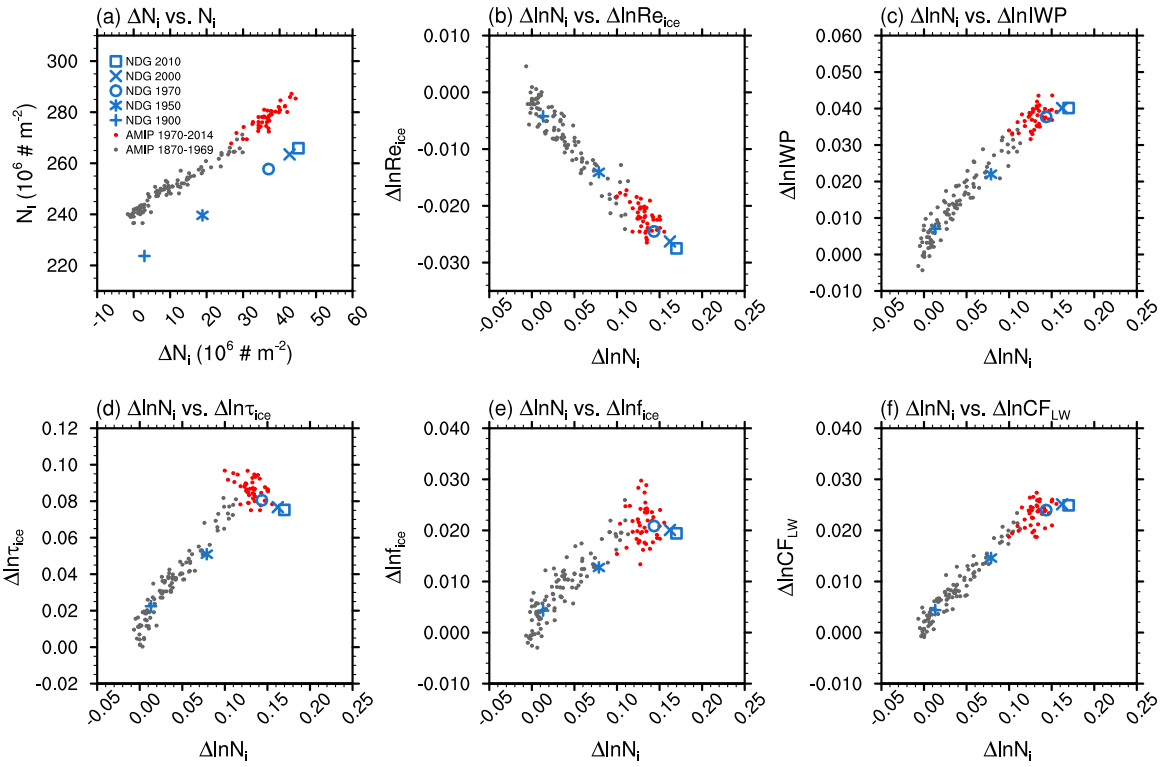

Figure S4: As Figure 9, but for relationships between ΔN_i and N_i, and between relative changes in N_i and other quantities. $\Delta lnX = \Delta X / X_{\mathrm{PD}}$. See section 4.4 for details.

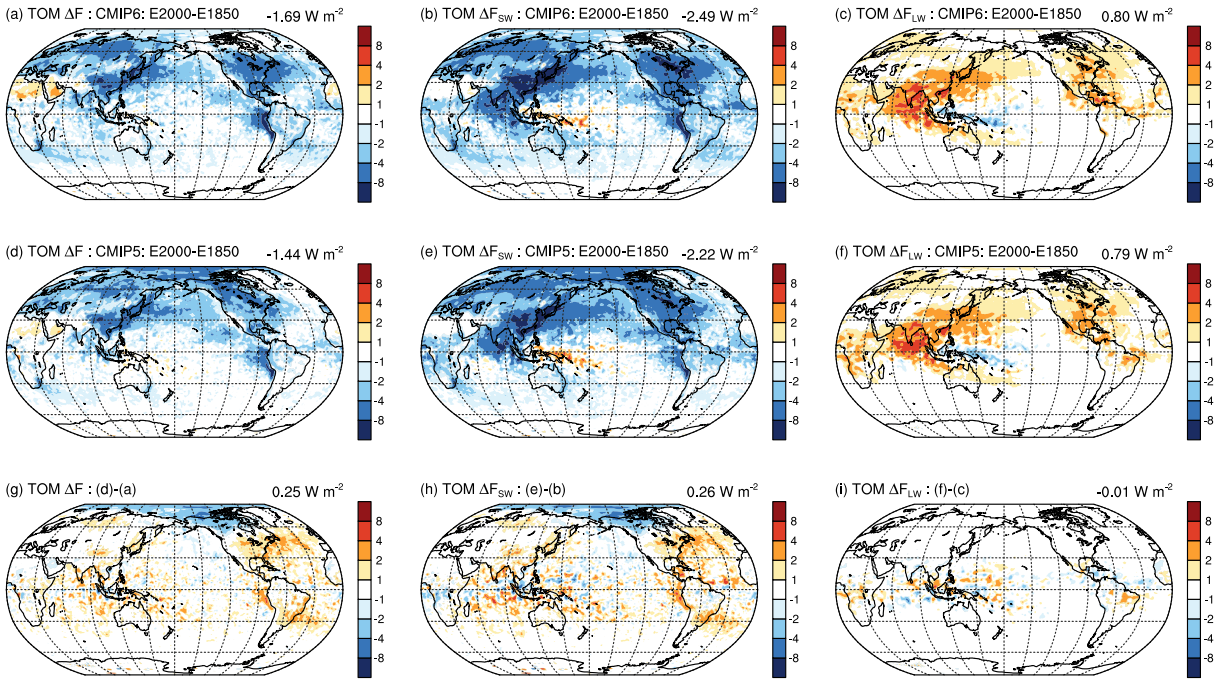

Figure S5: Annual mean global distribution of anthropogenic aerosol effects ($\mathrm{W\,m^{-2}}$) estimated with year 2000 CMIP5 (2nd row) and CMIP6 (1st row) emissions.

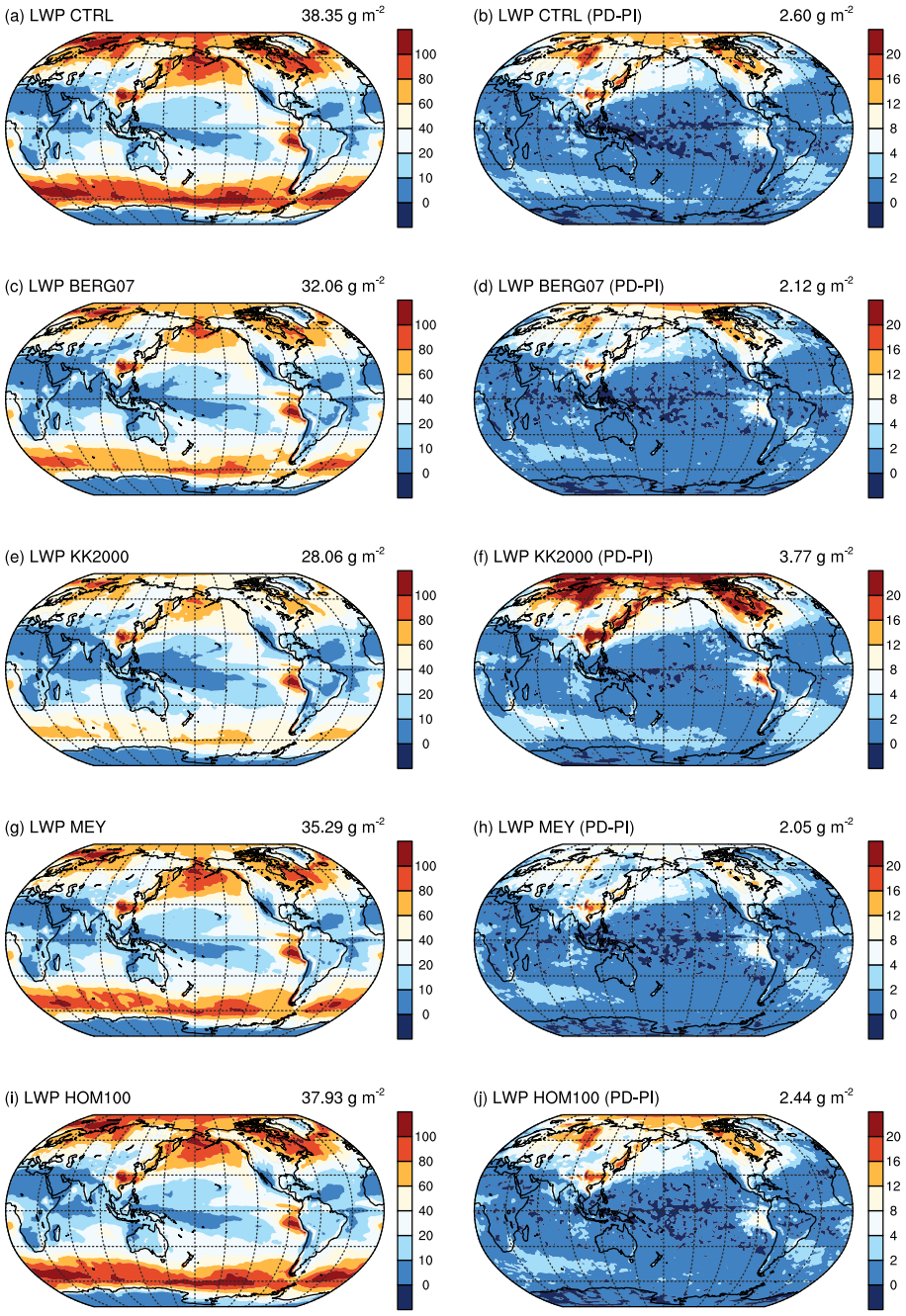

Figure S6: Annual mean global distribution of liquid water path and the sensitivity to aerosol perturbations ($\mathrm{W\,m^{-2}}$) in the reference and sensitivity simulations. See section 6 for details.

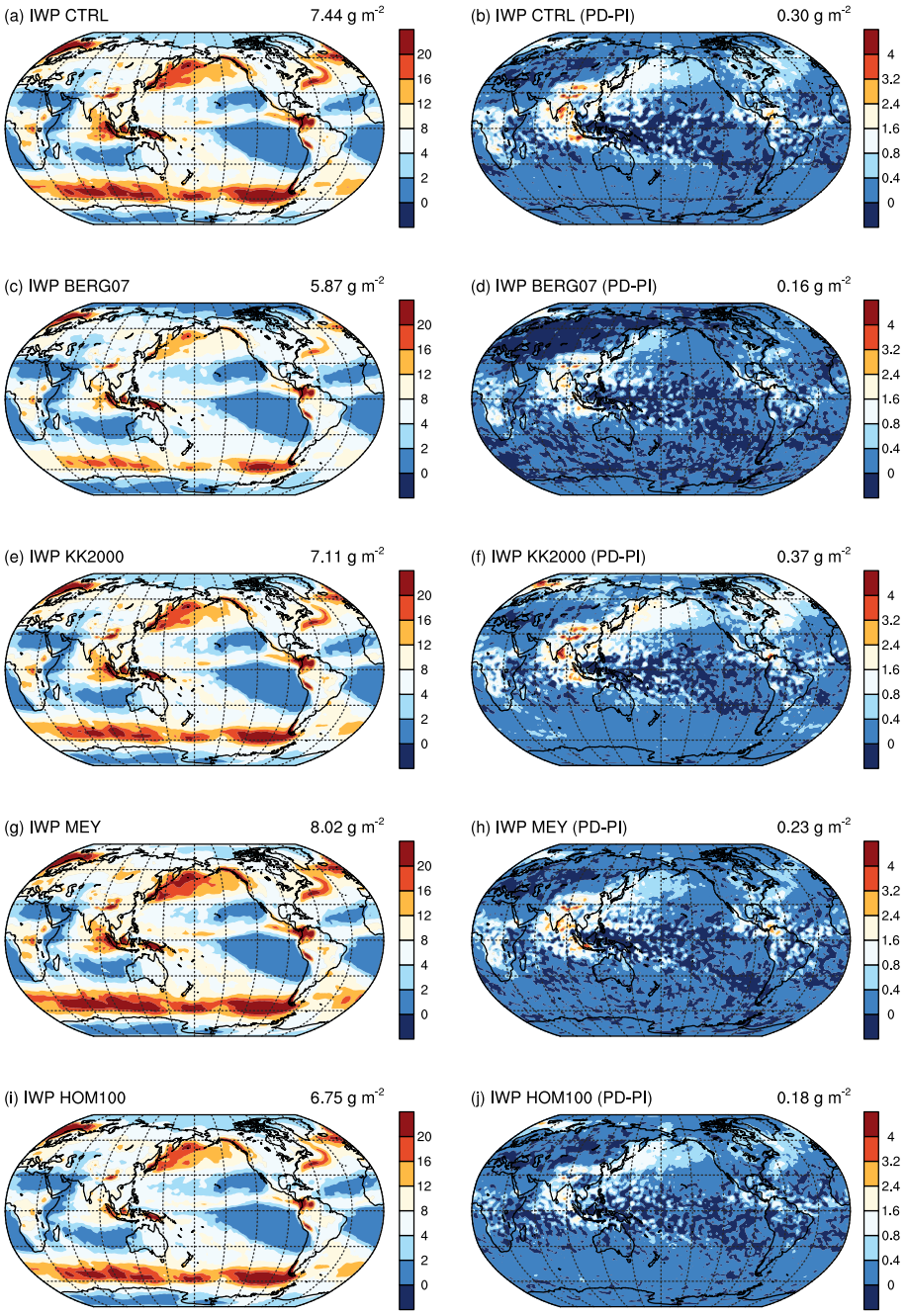

Figure S7: Annual mean global distribution of ice water path and the sensitivity to aerosol perturbations ($\mathrm{W\,m^{-2}}$) in the reference and sensitivity simulations. See section 6 for details.

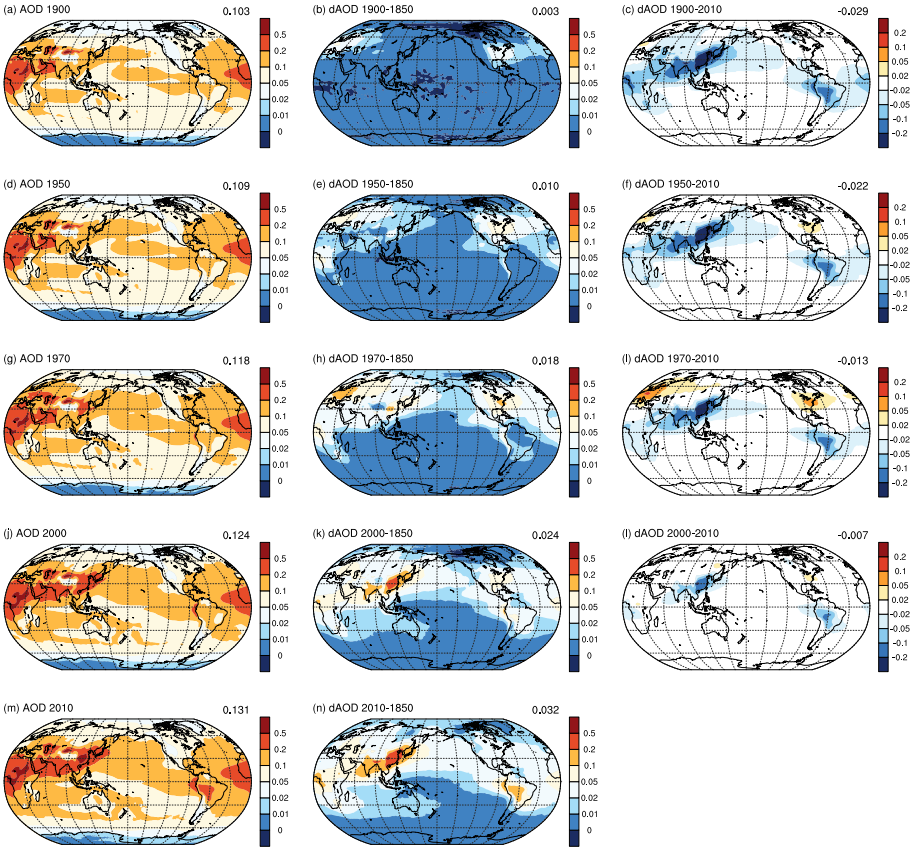

Figure S8: Annual mean global distribution of AOD in simulations with emissions for different years. See section 3.2 for details.

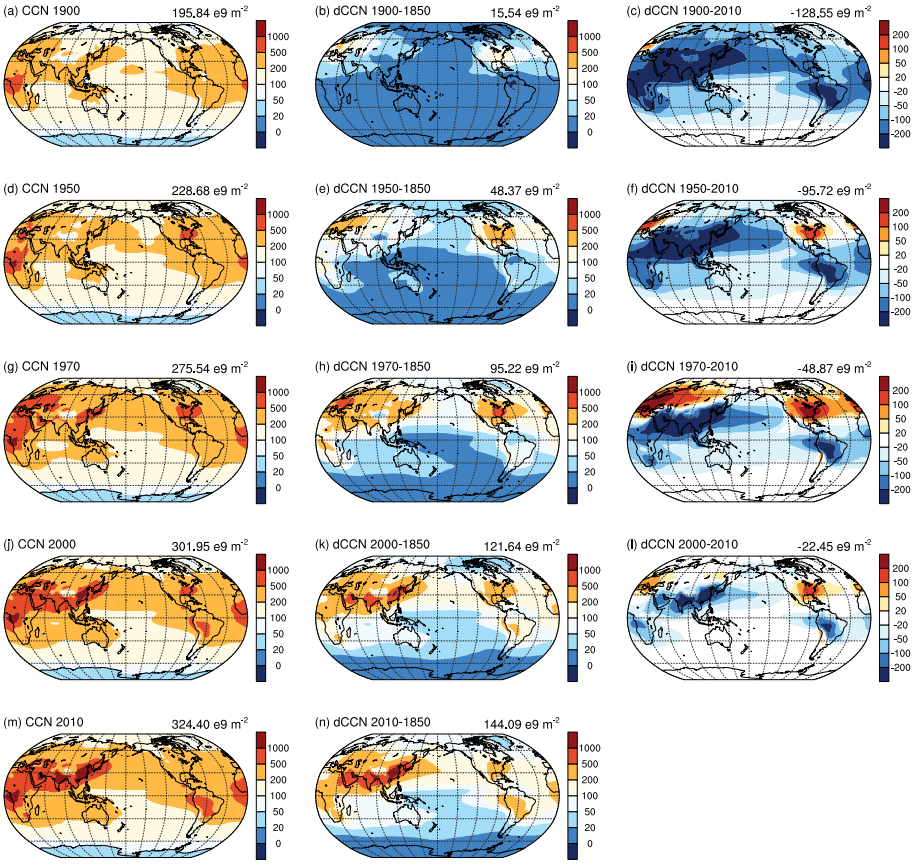

Figure S9: Annual mean global distribution of column-integrated CCN (at 0.1% supersaturation) concentrations in simulations with emissions for different years. See section 3.2 for details.

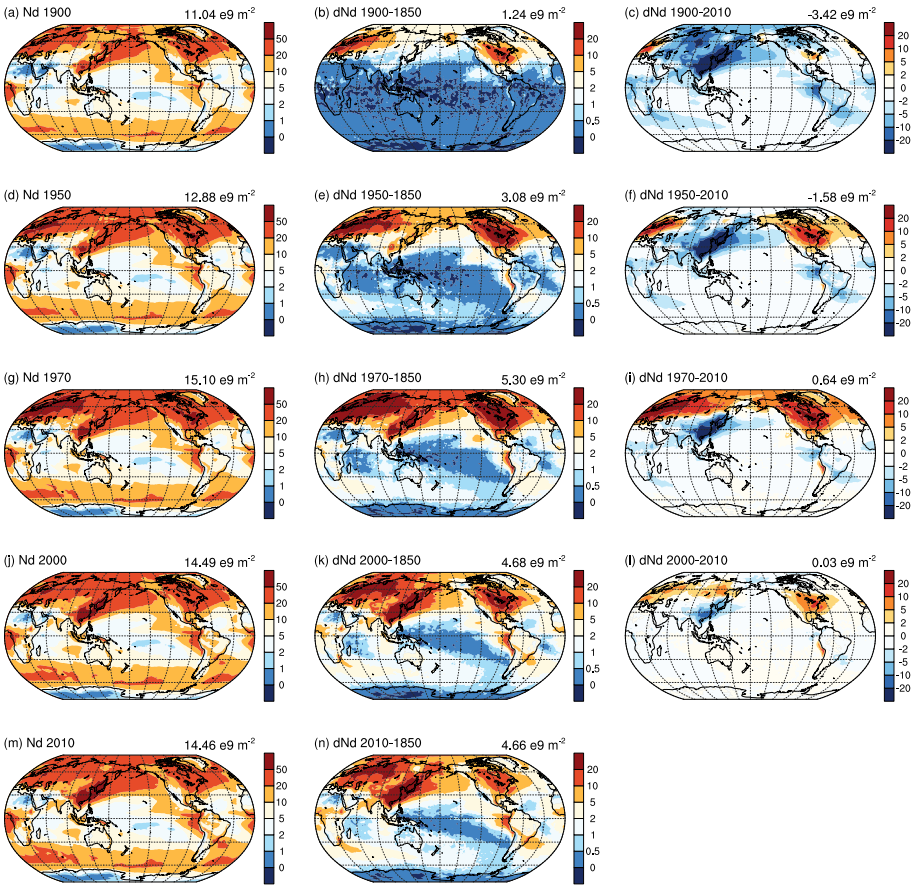

Figure S10: Annual mean global distribution of column-integrated cloud droplet number concentrations (N_d) in simulations with emissions for different years. See section 3.2 for details.

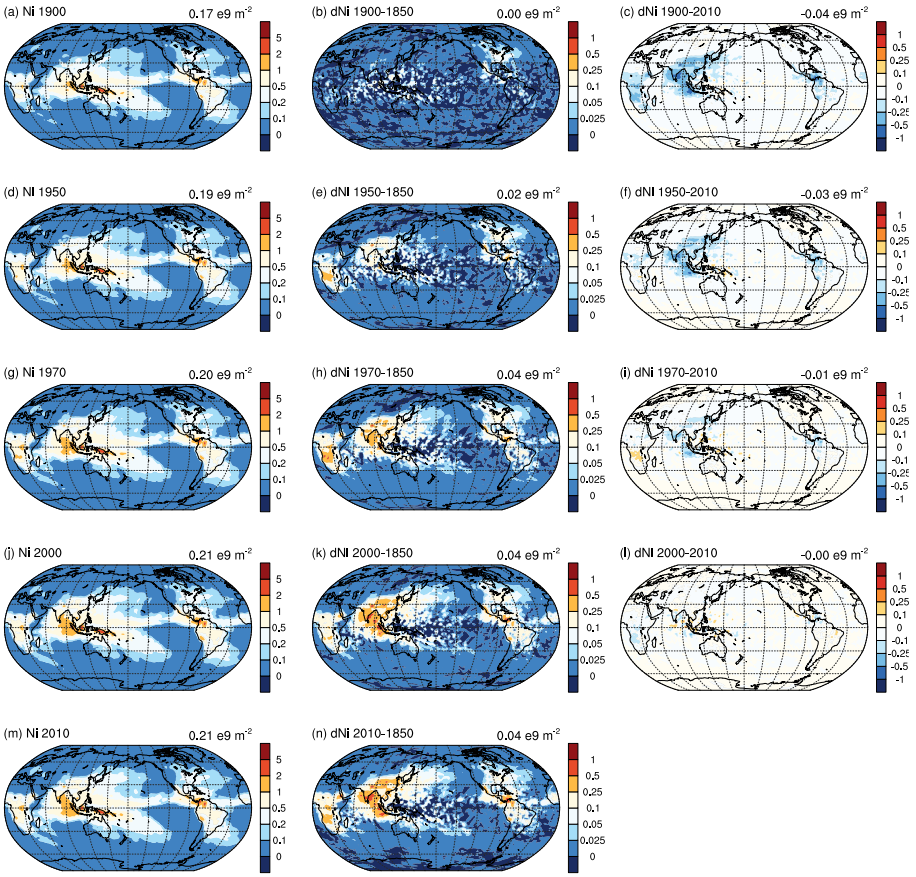

Figure S11: Similar as Figure S10, but annual mean global distribution of ice crystal number concentrations (N_i) vertically-integrated above 300hPa in simulations with emissions for different years. See section 3.2 for details.